ECS | The Electrochemical Society
Advancing solid state & electrochemical science & technology

Single Step Synthesis of Porous NiCoO$_2$ for Effective Electrooxidation of Glycerol in Alkaline Medium

View the article online for updates and enhancements.

Single Step Synthesis of Porous NiCoO$_2$ for Effective Electrooxidation of Glycerol in Alkaline Medium

Anchu Ashok,[1] Anand Kumar, [2,z] Janarthanan Ponraj,[3] Said A. Mansour,[3] and Faris Tarlochan[1]

[1]*Department of Mechanical and Industrial Engineering, College of Engineering, Qatar University, Doha, Qatar*
[2]*Department of Chemical Engineering, College of Engineering, Qatar University, Doha, Qatar*
[3]*Qatar Environment and Energy Research Institute (QEERI), Hamad Bin Khalifa University, Qatar Foundation, Doha, Qatar*

Herein, we report the electrooxidation of glycerol in alkaline media in presence of highly active and durable NiCoO$_2$ catalyst synthesized using single step solution combustion synthesis (SCS) and compare its activity with NiO and Co$_3$O$_4$ prepared using the same method. X-ray diffraction (XRD), X-Ray Photoelectron Spectroscopy (XPS), Scanning electron microscopy (SEM) with EDS and Transmission electron microscopy (TEM) along with EDS elemental/phase mapping were used to analyze the crystallinity, morphology and phase composition of the synthesized particles. TEM image with phase mapping confirms the existence of mixed NiCoO$_2$ and these materials shows enhanced performance when compared with individual metal oxides. The onset potential of NiCoO$_2$ is much lower and the oxidation current density obtained is relatively higher. More importantly, the current density and stability of NiCoO$_2$ obtained from chronoamperometry makes it a promising catalyst for glycerol based fuel cells.

During last decades, the electrooxidation of small organic molecules such as C$_1$ (methanol), C$_2$ (ethanol and ethylene glycol) and C$_3$ (glycerol) alcohols has been attained great interest because of their potential application in direct alcohol fuel cells (DAFCs).[1–4] Early stages researchers found interest in developing methanol and ethanol fuel cells as a power source for the commonly used portable devices due to its higher energy density and improved efficiency of liquid fuels than gaseous fuels such as hydrogen. However, the higher toxicity of methanol limits its application when compared to ethanol. Later, the development of ethanol-based fuel cells also reduced the research interest due to the difficulty of breaking C-C bond for the complete electrooxidation at lower temperature. Recent studies are progressing toward establishing polyhydric alcohols such as glycerol and ethylene glycol based fuel cells that are less toxic than methanol, have higher boiling point and low volatility, and possess relatively higher theoretical energy density.[5,6] Glycerol is obtained as a by-product during the conversion of oil and through biomass into biodiesel.[7] A rapid increase in the production of biodiesel increases the production of glycerol making it surplus in market and driving its application as a feedstock targeting new reactions such as electrooxidation process. Due to the molecular structural complexity of glycerol when compared to other C$_1$ and C$_2$ alcohols the electrooxidation is more challenging. In spite of these challenges, glycerol electrooxidation is developed as a simple approach for generation of electricity and co-synthesis of many value-added products as intermediates that includes glycerates, oxalates, tartronate, glycolate, dihydroxyacetone, mesoxalate, hydroxypyruvate and formate ions.[8–11] Some of these intermediates are used as drug delivery agents, polymer precursors and heavy metal complexing agents in industries. Tartronic acid has the second highest selectivity in the electrooxidation processes, is one of the commonly used very expensive chemicals in medical practices.

It is necessary to develop an anode electrocatalyst with better activity and performance that can completely electrooxidize glycerol to CO$_2$ at low over potentials. The anode catalyst should possess high activity for the for C-C-C bond cleaving and must have high resistance to the poisoning by carbon monoxide (CO) as reaction intermediate. Pt, Pd, Au and its alloys are well common anode catalysts for the electrooxidation of small organic molecules. Kim et al. reported the electrocatalytic oxidation of glycerol and ethylene glycol over PtAg nanotubes as anode catalysts and achieved an enhanced performance when compared with Pt nanotube and commercial Pt/C based on the peak current density, lower onset potential and improved anti-poisoning.[12] Wei Hong and co-workers synthesize trimetallic PdRuCo hollow nanocrystals using simple one-pot method with different composition and tested its activity toward electrooxidation of ethylene glycol and glycerol and found to be more comparable with commercial Pd/C.[13]

Owing to the sluggish kinetics, CO poisoning and high costs; Pt and Pt alloys are not suitable for large-scale commercial applications. Increasingly, current researchers are focusing on to replace the noble metals with alternative materials that are cheaper, readily available and non-toxic while maintaining the high activity and stabile performance. Nickel and its bimetals are most commonly used non-Pt group metals (non-PGMs) electrocatalysts that are suitable for many electrochemical performances such as fuel cells, batteries and supercapacitors.[14–16] Jian-Hua et al. synthesized three dimensional Au/Ni/Polystyrene spheres that shows excellent performance for the electrooxidation of glycerol.[17] Oliveira et al. reported the glycerol conversion over carbon supported Ni based catalyst and identified the reaction intermediates and products using in situ FTIR measurement.[18] B. Habibi and N. Delnavaz studied the electrooxidation of glycerol over Ni and its alloy (Ni-Cu and Ni-Co) nanoparticles modified carbon-ceramic electrodes in 1M NaOH and found that alloyed particles are more catalytically active than Ni mono-metal.[19] Recently, Houache and researchers tested the glycerol electrooxidation on un-treated Ni surface and Ni-surface treated in ascorbic acid using sin-wave.[20] They studied the effect of treatment on the surface characteristics of Ni and correlated its electrochemical properties. The Ni-treated surface gave an increased surface area of six-folds enhancing current density up to nine times.[20] In addition to Ni, cobalt and cobalt oxides are also reported to be active for thermal-catalytic and electro-catalytic conversion of alcohols and fuel cell based applications.[21–23] In many cases, bimetals, alloys and mixed metal oxides of transition metals are found to be more active compared to their individual metal (oxide) constituents.[19,21,24] Our objective is to take advantage of these two active metals (- oxides) of Ni and Co, and synthesize a mixed metal oxide using a technique such as solution combustion synthesis to give high surface area for effective electro

oxidation.[21–27] It will contribute toward the global research efforts on reducing the cost of catalysts by minimizing the noble metal loading with non-PGMs.

In this work, we report the synthesis of mixed Ni-Co oxides and its monometals that are investigated toward the electrooxidation of glycerol. $NiCoO_2$ was successfully synthesized using a single step combustion synthesis method that is fast, economical and simple to operate. The combustion temperature, amount of fuel used, evolution of gases are the main parameters in solution combustion synthesis that control the morphology, size and uniformity of nanoparticles. Detailed explanation on the synthesis method are reported in our previous works.[21–27] In summary, by increasing the amount of fuel during synthesis, the environment becomes more reducing in nature and releases more gas phase products during combustion. While, combustion temperature is a function of the exothermicity of the reaction, the nature of product (whether metallic or oxide phase) and porosity are affected as the synthesized metal oxide gets further reduced whereas simultaneously the escaping gases create more porous structure.[21–27]

Experimental

Synthesis method.—The $NiCoO_2$ was prepared from the aqueous solution of 5.83 g of nickel nitrate ($Ni(NO_3)_2 \cdot 6H_2O$), 5.84 g of cobalt nitrate ($Co(NO_3)_2 \cdot 6H_2O$) and 1.667 g glycine ($C_2H_5NO_2$) using solution combustion synthesis with a fuel to oxidizer ratio of 0.5. The precursor amounts were calculated on the basis to synthesize 3 g of nanopowders in the output following the stoichiometric calculations reported previously.[21–27] The measured reagents were dissolved in 25 ml of ultrapure water and stirred continuously using hand to obtain a homogeneous mixture. This homogeneous solution was placed over the hot plate (Barnstead Thermolyne model no 46925) at 250°C until the water the gets evaporated, followed by self-ignition that triggers the combustion reaction inside the beaker converting the precursors into desired nanoparticles (NPs). NPs thus obtained were crushed with a hand mortar and sieved using a 100 μm sieve to obtain uniform particles.

Synthesized nanoparticle was mixed with Vulcan carbon to ensure the conductivity during electrochemical measurement. A 0.03 g of catalyst was added to 0.2 ml of DI water and sonicate for 1 hr for the complete dispersion and a 0.07 g of Vulcan carbon was slowly added to the catalyst that was sonicated again for 1 hr for the complete impregnation of catalysts on carbon. The ink formed was heated to 110°C and the dried sample was crushed and sieved again to obtain the electrocatalyst. A 0.01 g of thus obtained electrocatalyst was dispersed in 2.5 ml of DI water and sonicate for 1 hr. A 20 μl of this solution was dropped over a glassy carbon disc with 5 mm diameter connected with the Teflon- RDE housing and let it for drying overnight. Again a 20 μl of 0.1% nafion solution was dropped over it to bind the catalyst over the electrode and this can be used as a working electrode.

Material characterization.—Rigaku MiniFlexII Desktop X-ray powder diffractometer using Cu-Kα radiation using 10–80-degree 2ϑ scan range was used to identify the crystalline phases. The bonding configuration and elemental analysis on the surface of bimetallic materials were identified using X-Ray Photoelectron Spectroscopy (XPS, Kratos AXIS Ultra DLD). FEI Nova Nano 450 SEM equipped with EDS elemental analyzer was used to study sample surface morphology. FEI Talos F200X TEM coupled with FEI SuperX EDS system was used to identify particle sizes and elemental mapping. The sample for the TEM analysis was prepared by dispersing the nanoparticles in DI water and sonicating for 30 minutes. A 20 μl of the dispersed solution was dropped slowly over the 200 mesh copper/carbon grid and dried at room temperature before analysis.

Electrochemical characterization.—Cyclic voltammetry (CV), linear Sweep voltammery (LSV) and chronoamperometry (CA) are the three main electrochemical experiments that are measured us-
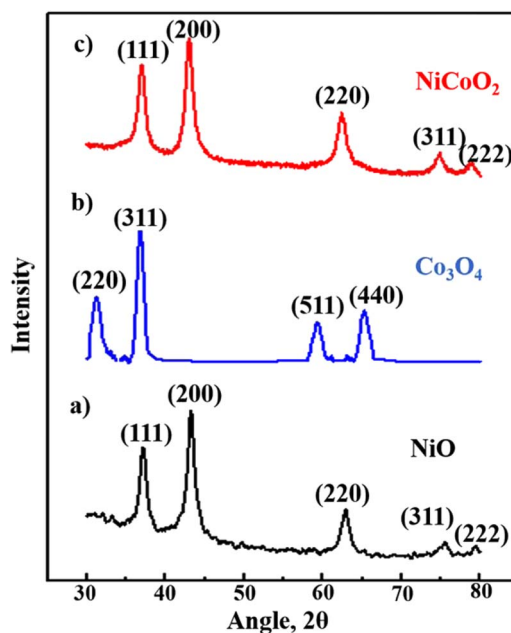

Figure 1. XRD patterns of (a) NiO, (b) Co_3O_4 and (c) $NiCoO_2$.

ing PINE instruments bipotentiostat (WaveDriver 20) with a standard three-cell electrode system in 1M KOH electrolyte and 0.1 M glycerol. A Teflon- RDE housing with 5 mm diameter glassy carbon was used as a working electrode. A platinum coil and and Ag/AgCl were used as counter electrode and reference electrode respectively. The electrolyte of 1 M KOH was purged using pure N_2 prior to the experiment. The working electrode was pre-treated with a scan rate of 500 mV/s in the potential window of −0.9 V to 0.6 V for 100 segments. The CV of N_2 saturated 1M KOH was measured in presence of catalyst in the potential range of −0.9 V to 0.6 V before conduction the electrooxidation experiments. The solution was changed to 1 M KOH+ 0.1 M glycerol and purged with N_2 for 1 hr and conducted the electrooxidation of glycerol. LSV was measured at a rotational speed of 300 rpm in the same potential range where CV was measured. The long-term electrolysis of glycerol was measured using chronoamperometry at a fixed potential for 3600 sec.

Results and Discussion

The crystal structures of the monometal oxides and mixed metal oxides ($NiCoO_2$) were characterized using XRD technique as shown in Fig. 1. The XRD pattern of NiO in Fig. 1a shows major peaks at 37.2°, 43.2°, 62.8°, 75.5° and 79.5° corresponding to (111), (200), (220), (311) and (222) that are indexed to face-centered cubic phase of NiO (JCPDS card no. #47-1049). In the XRD pattern in Fig. 2b cubic type Co_3O_4 nanoparticle formation was confirmed based on JCPDS card no. # 042-1467. Fig. 1c shows five distinct diffraction peaks at 36.8°, 42.82°, 61.7°, 73.9° and 77.9° respectively that are ascribed to (111), (200), (220), (311) and (222) crystal planes with cubic $NiCoO_2$ (JCPDS card no. # 10-0188). No other peaks of monometallic oxides (NiO or Co_3O_4) are detected in Fig. 1c, indicating the presence of highly pure $NiCoO_2$ without any kinds of impurities.

The xps survey spectrum shown in Fig. 2a in the range of 0–1000 eV confirms the existence of Ni, Co and O in $NiCoO_2$ synthesized using solution combustion method. In Fig. 2b, there are two main spin orbitals at 854.6 eV and 871.7 eV corresponds to the presence of Ni $2p_{3/2}$ and Ni $2p_{1/2}$ along with two satellite peaks at 860.23 eV and 878.3 eV.[28,29] The deconvolution of the main spin orbitals in Ni 2p shows the presence of divalent oxidation states (Ni^{2+} and Ni^{3+}) of Ni in $NiCoO_2$. Co 2p spectrum in Fig. 2c consist of two main peaks
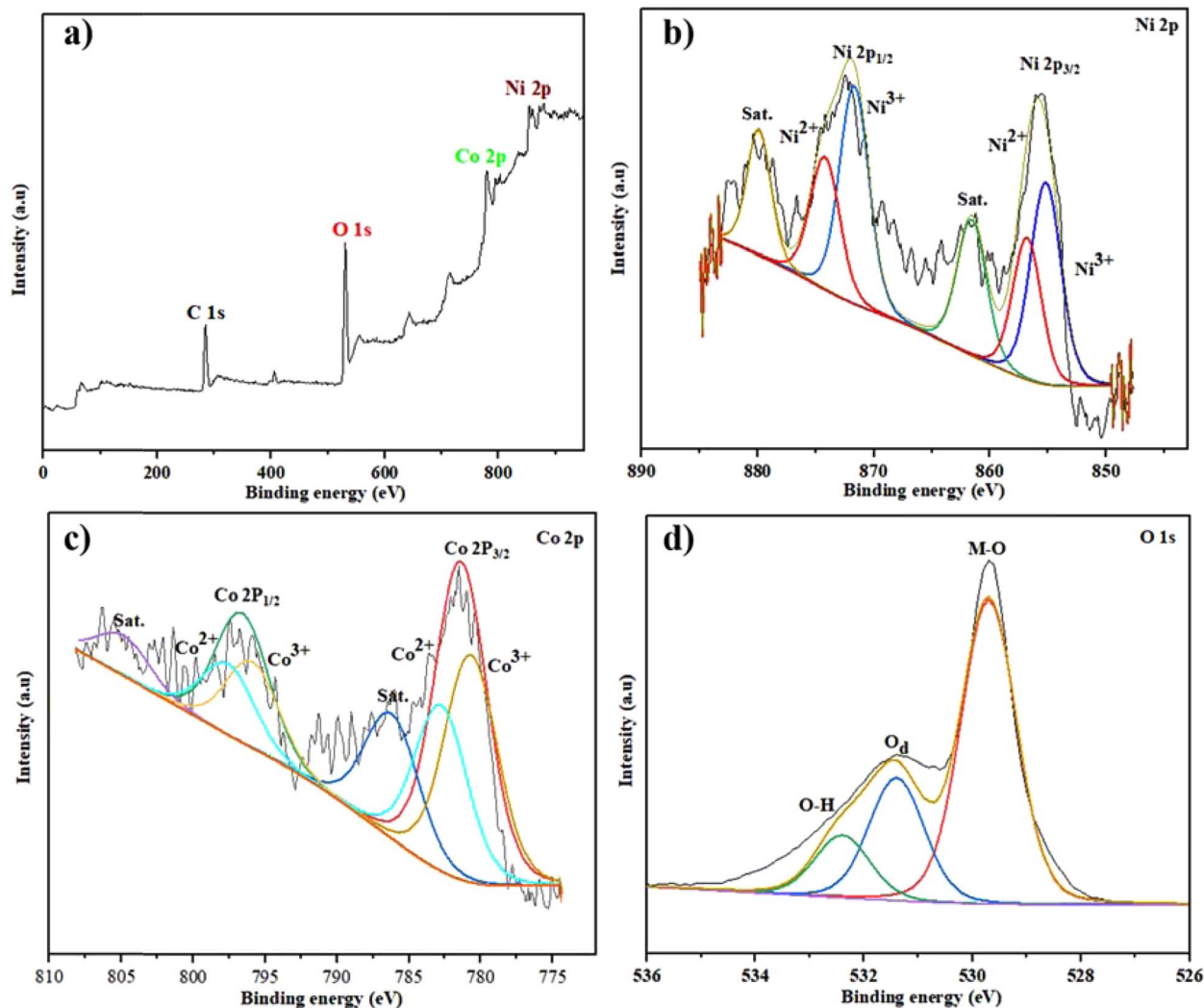
Figure 2. XPS spectra of (a) survey scan (b) Ni 2p (c) Co 2p and d) O 1s of NiCoO$_2$.

at 780.12 eV (Co 2p$_{3/2}$) and 796.23 eV (Co 2p$_{1/2}$) with a separation of 16 eV.[30] The presence of two satellite peaks in Co 2p is indicated as "Sat.". The O1s deconvolution spectrum in Fig. 2d shows the presence of 3 peaks and the main characteristic peak at 529.8 eV attributed to the oxygen bonded to the metals (Ni and Co). The peaks at 531.2 and 532.8 eV is due to the defect sites with oxygen vacancy and the presence of oxygen containing species (O-H) on the surface.[31] The quantitative analysis of each element on the surface indicates elemental composition to be in the ratio of Ni: Co: O: C to be 5.21: 7.06: 36.88: 60.85. It should be noted that XPS is primarily a surface analysis technique and bulk composition could differ from surfaces as a result of surface rearrangements and restructuring.

Fig. 3 shows the SEM images of monometallic and bimetallic oxides of nickel and cobalt. All samples show clear porous structures typically obtained during combustion synthesis. To identify the distribution of elements in the sample, the elemental analysis of Ni, Co and O using EDS was conducted of the sample shown in Fig. 3c. In NiCoO$_2$, the average atomic concentration of Ni, Co and O are 17.09, 18.19 and 47.33 respectively that are in the ratio of approximately around 1:1:3. In order to remove the carbon content, the synthesized catalysts was treated at 400°C for 2 hr inside a horizontal tubular furnace in presence of continuous flow of O$_2$ gas. The EDX analysis of the resulted compound contains Ni, Co and O in atomic concentration (%) of 26.3, 28.6, 44.8 respectively, which is much closer to atomic ratio expected in NiCoO$_2$.

The TEM images in Fig. 4a shows the presence of ultrafine porous NiCoO$_2$ particles with irregular morphology. The whole area was composed with many small NiCoO$_2$ particles that are connected to form a mesoporous sheet like morphology. The lattice spacing of 0.24 nm and 0.21 nm corresponding to the crystal planes (111) and (200) of NiCoO$_2$ shown in Fig. 4b, which is consistent with the XRD results in Fig. 1. Elemental mapping of Ni, Co, O and Ni-Co using energy dispersive spectroscopy (EDS) identified the distribution of sample elements. It is clear from Fig. 4d that Ni, Co and O are well dispersed and uniformly distributed throughout the area of the sample. The EDS analysis indicates Ni and Co to be in approx. 1:1 atomic ratio. From the TEM elemental mapping, SEM analysis and XRD confirmed the existence of NiCoO$_2$ in the catalysts that was further evaluated for electrochemical characterization explained below.

The electrochemical catalytic activity of NiCoO$_2$ was studied and compared with NiO and Co$_3$O$_4$ using cyclic voltammetry (CV) technique. Fig. 5 shows the CV of Ni/C, Co$_3$O$_4$/C and NiCoO$_2$/C catalysts in N$_2$ saturated 1M KOH at a scan rate 50 mVs^{-1} in the potential range of −0.9 V to 0.6 V. The current-voltage profile of Ni/C in Fig. 5a shows the dominant double layer region between −0.9 V and 0.25 V. During forward scan, the anodic peak at 0.42 V indicates the presence of nickel hydroxide that covered over the electrode surface.[18]
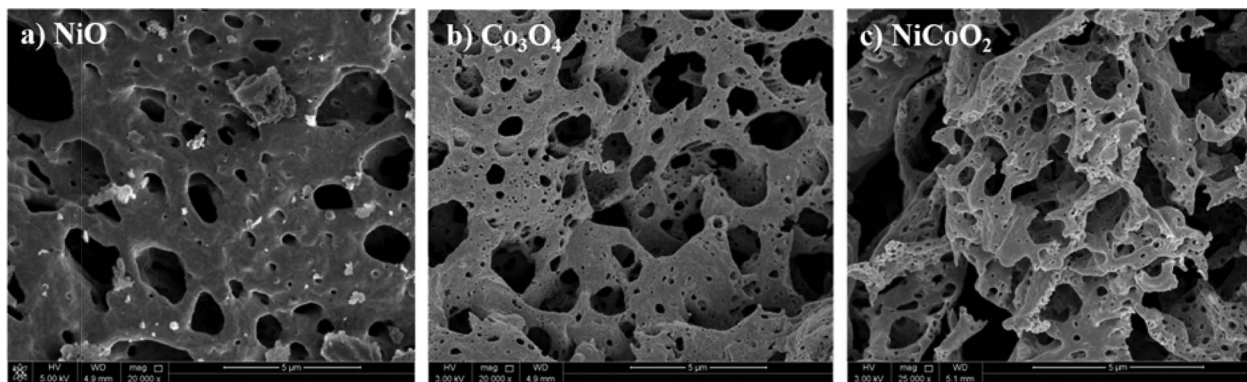
$$Ni + 2OH^- \rightarrow Ni(OH)_2 + 2e^- \qquad [1]$$
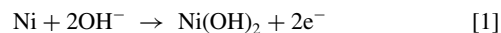
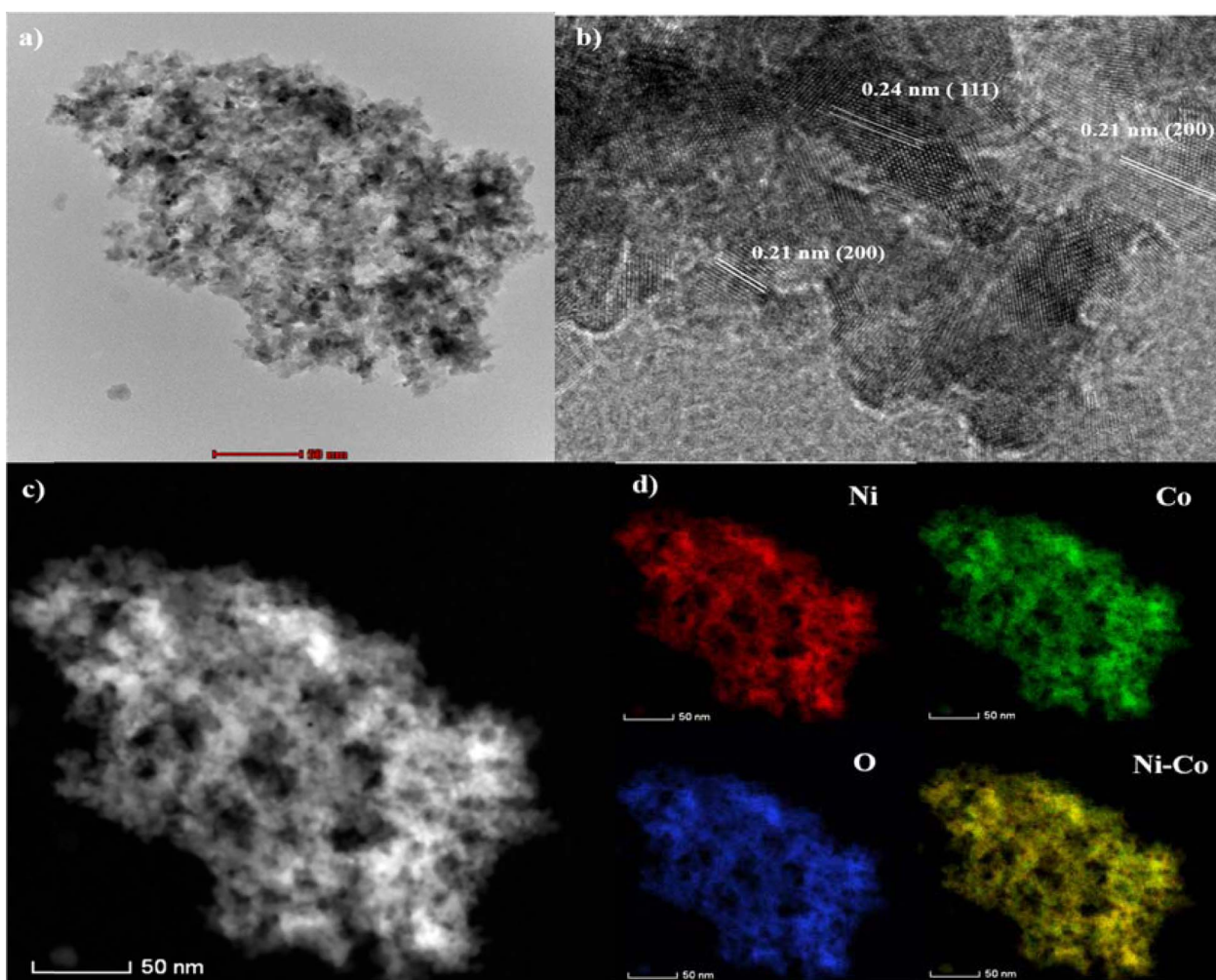**Figure 3.** SEM micrographs of a) NiO, b) Co_3O_4, and c) $NiCoO_2$.

Figure 4. a) Low magnification TEM image, b) High resolution TEM (HRTEM) image, c) STEM image, d) Elemental mapping by high-angle annular dark-field scanning transmission electron microscopy (HAADF-STEM) of Ni, Co, O and Ni-Co in $NiCoO_2$ catalysts.

At higher potential, there is a formation of redox couple Ni(II)/Ni(III) according to the equation below

$$Ni(OH)_2 + OH^- \leftrightarrow NiOOH + H_2O + e^- \qquad [2]$$

At lower potential of anodic scan, the Ni catalyst on the electrode can be easily oxidized to α-Ni(OH)$_2$ as shown in Equation 1. And with rise in potential, more hydrated α-Ni(OH)$_2$ was converted to β-Ni(OH)$_2$ that are comparatively more stable but less hydrated. This process was irreversible due to the high stability of β-Ni(OH)$_2$ and the conversion to α-Ni(OH)$_2$ or Ni was not possible.[18–20] At higher potential the β-Ni(OH)$_2$ made a preferable conversion to NiOOH as shown in Equation 2. The cathodic peak in the reverse scan at 0.38 V(a$_1$) corresponds to the reversible electrooxidation of Ni(OH)$_2$ to Ni phase.
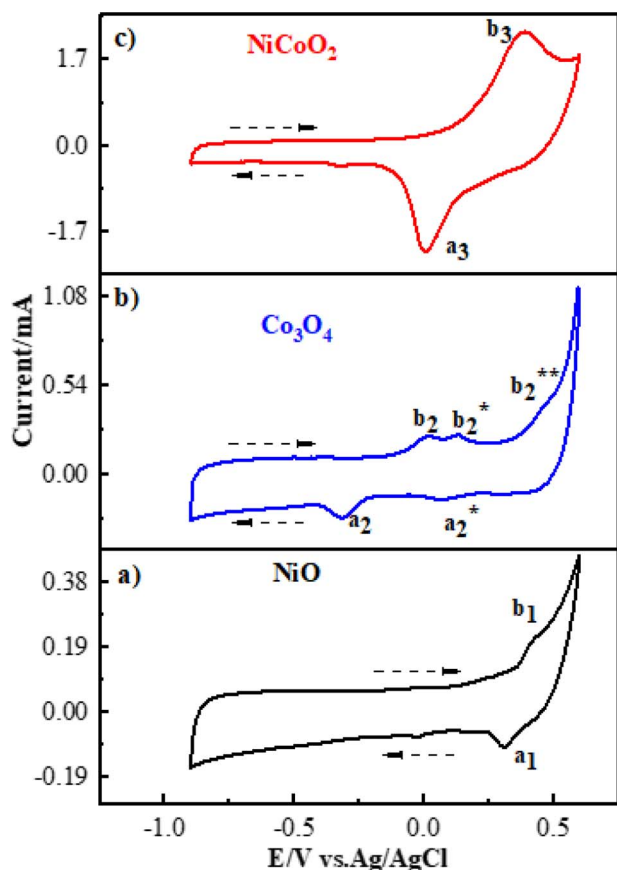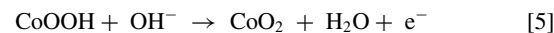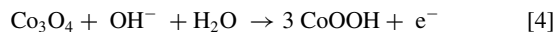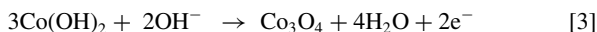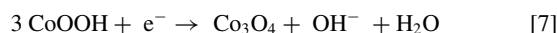
Figure 5. Cyclic voltammograms of a) NiO/C, b) Co_3O_4/C, and c) $NiCoO_2$/C in N_2 saturated 1M KOH solution with a scan rate of 50 mVs^{-1}.

Fig. 5b shows the CV of Co_3O_4/C with multiples anodic/cathodic peak at different potential indicates the formation of various cobalt species with different oxidation states.[26,32] During the forward scan, the anodic peaks b_2^*, b_2^{**}, b_2^{***} corresponds to the following reactions

$$3Co(OH)_2 + 2OH^- \rightarrow Co_3O_4 + 4H_2O + 2e^- \qquad [3]$$

$$Co_3O_4 + OH^- + H_2O \rightarrow 3\,CoOOH + e^- \qquad [4]$$

$$CoOOH + OH^- \rightarrow CoO_2 + H_2O + e^- \qquad [5]$$

Similarly, the cathodic reaction involved in Co_3O_4/C can be represented as

$$CoO_2 + H_2O + e^- \rightarrow CoOOH + OH^- \qquad [6]$$

$$3\,CoOOH + e^- \rightarrow Co_3O_4 + OH^- + H_2O \qquad [7]$$

$$Co_3O_4 + 4H_2O + 2e^- \rightarrow 3Co(OH)_2 + 2OH^- \qquad [8]$$

During this redox reaction of $Co(OH)_2/Co_3O_4$, $Co_3O_4/CoOOH$, $CoOOH/CoO_2$, cobalt undergo different charge transfer reactions in the form of $Co(II) \leftrightarrow Co(III) \leftrightarrow Co(IV)$. The addition of this Co along with NiO in $NiCoO_2$ cause some changes in redox reaction peaks as shown in Fig. 5c. The anodic oxidation and cathodic reduction peak position of $NiCoO_2$ are now at lower positive potential than NiO and Co_3O_4. The peak current of the redox reactions is also comparatively higher for $NiCoO_2$ than its monometallic oxides. This could be due to the formation of $Co(OH)_2$ from the Co prior to the $Ni(OH)_2$. The possible redox reaction M-O/M-O-OH (M be Ni or Co) on $NiCoO_2$ surface can be represented as

$$NiCoO_2 + 2OH^- \leftrightarrow NiOOH + CoOOH + 2e^- \qquad [9]$$

The redox peaks correspond to NiOOH and CoOOH overlap together and form a single peak in $NiCoO_2$ is possible only through the proper alloying of Ni and Co species in the catalyst that will also enhances its catalytic property.[33,34] These catalysts are tested toward the glycerol electrooxidation as presented in the following sections.

The cyclic voltammogram of glycerol electrooxidation on NiO, Co_3O_4 and $NiCoO_2$ supported with carbon in 0.1 M glycerol is shown in the Fig. 6a. Based on the previous reports, it is clear that glycerol electrooxidation superimposed with the transformation of $Ni(OH)_2$ to NiOOH and cause the replacement of anodic peak (b1) in NiO/C with a smooth curve. During the reverse scan, the reduction peak (NiOOH→$Ni(OH)_2$) a_1 (Fig. 5a) is completely disappeared in glycerol electrooxidation of NiO/C (Fig. 6a). This could be due to the indirect electron transfer mechanism that completely consumes NiOOH
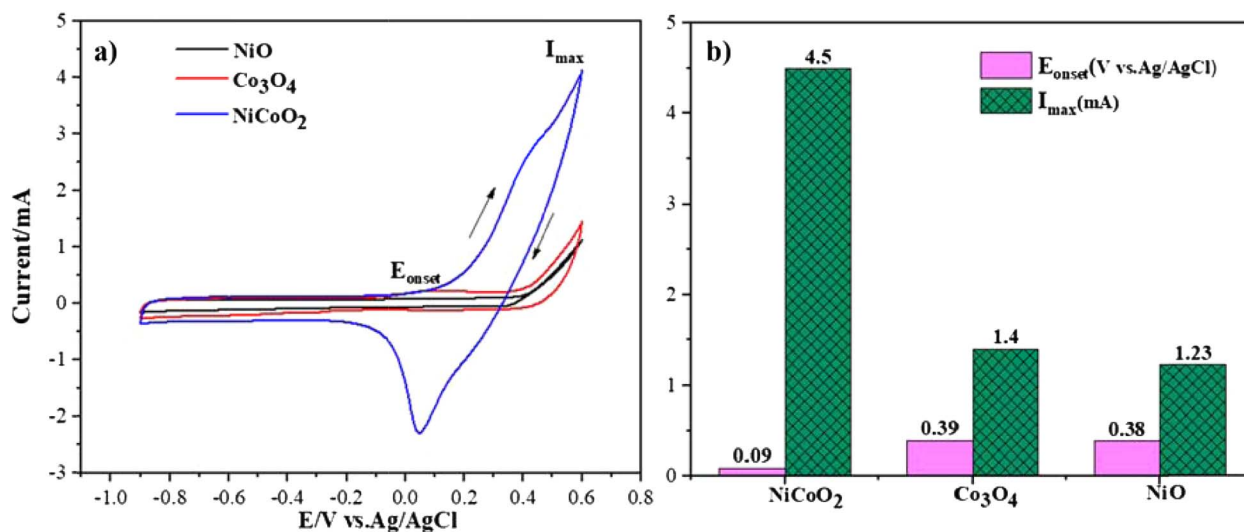

Figure 6. a) Cyclic voltammogram of NiO/C, Co_3O_4/C and $NiCoO_2$/C in 0.1 M glycerol + 1M KOH at a scan rate of 50 mVs^{-1}, b) Onset potential and current density of all the three catalysts in glycerol electrooxidation.
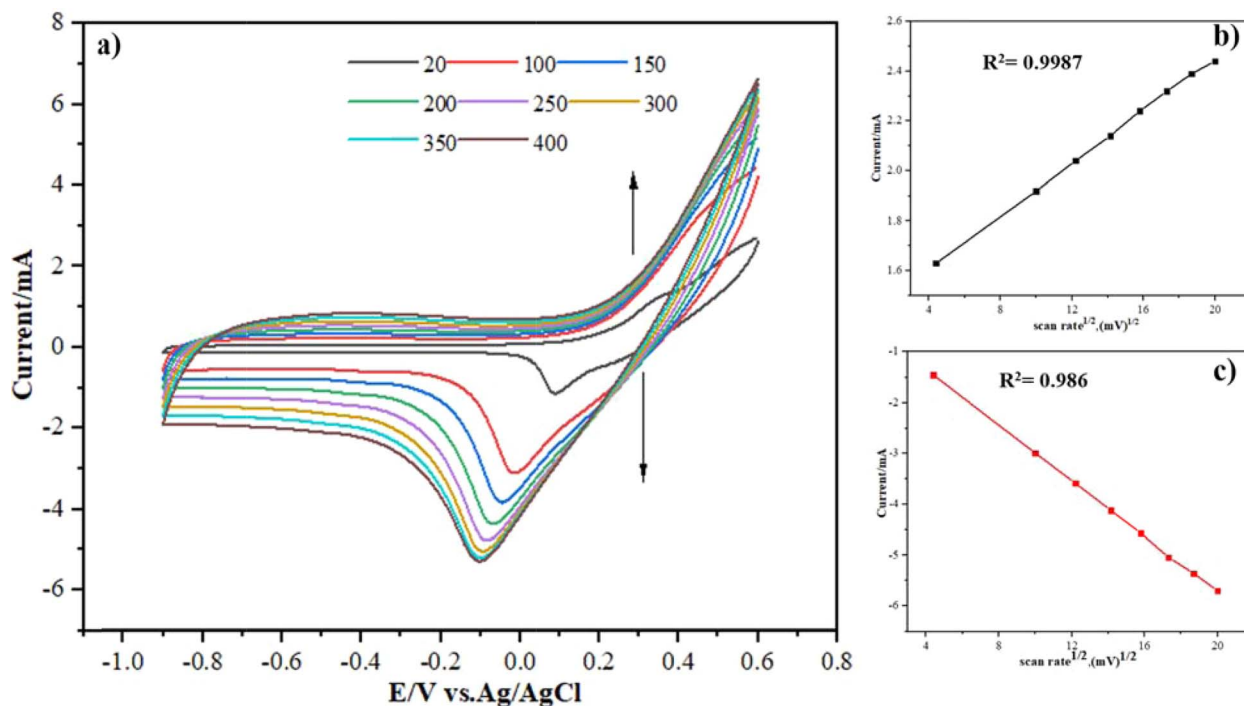
Figure 7. a) Effect of scan rate on the electrooxidation of glycerol in NiCoO$_2$ at 0.1 M Glycerol + 1M KOH, b) the dependence of anodic peak current on the square root of scan rate, c) the dependence of cathodic peak current on the square root of scan rate.

during the glycerol oxidation and forms Ni(OH)$_2$ and that was first reported by Fleischmann and co-workers during the alcohol electrooxidation of Ni surface in alkaline medium.[35]

The glycerol oxidation reaction on the NiO/C electrode can be represented as

$$NiOOH + C_3H_8O_3 \rightarrow Ni(OH)_2 + Products \qquad [10]$$

During this reaction the glycerol is oxidized to intermediate products and NiOOH is reduced to Ni(OH)$_2$. The glycerol oxidation completely removes the NiOOH from the electrode surface and the reduction of NiOOH to Ni(OH)$_2$ in the reverse scan is impossible.

Apart from this indirect electron transfer, there is another direct mode of electron transfer reported in glycerol oxidation.[36,37] In that case, the glycerol molecules penetrate Ni(OH)$_2$ surface and are oxidized using the hydroxide ions that are on the surface. The reduction peak remains there, as the NiOOH is not completely used in this reaction. The vanishing of reduction peak in our result shows that the NiO/C follows an indirect electron transfer reaction in the glycerol oxidation. The lower onset potential and higher current at 0.6 V for NiCoO$_2$ with respect to NiO and Co$_3$O$_4$ indicates the enhanced electrocatalytic activity for glycerol electrooxidation. The effect of scan rate on the glycerol electrooxidation of NiCoO$_2$ is shown in Fig. 7a. The anodic and cathodic peak currents of glycerol oxidation on forward and reverse scan are represented as being proportional to the square root of scan rate. It is clear that the anodic and cathodic peak currents increase with scan rate and it has a linear relation with square root of scan rate (mV)$^{1/2}$. This indicates the existence of electron transfer mechanism in NiCoO$_2$ electrode being controlled through the diffusion process.[19] Apart from that, the anodic peak shows a positive shift whereas the cathodic peak experiences a negative shift with an increase in the scan rate in NiCoO$_2$ indicating an irreversible glycerol electrooxidation on the catalyst surface.

The kinetic parameters of the catalysts toward glycerol electrooxidation was identified using Tafel plot with applied voltage on y-axis

and log(current) on x-axis as represented below:

$$\eta = b \, log \frac{i}{i_0} \text{where b} = \frac{2.3RT}{n\alpha F} \qquad [11]$$

where η is the overpotential, b is the Tafel slope, i is the measured current, i_0 is the exchange current density, n be the overall electron transfer in the oxidation reaction, α is the charge transfer coefficient, T is the temperature in Kelvin, R and F are the universal gas constant and Faraday constant respectively. The value of b can be measured from the slope of the linearly fitted portion of Tafel region. The obtained Tafel slope for NiO, Co$_3$O$_4$ and NiCoO$_2$ are 224 mV dec^{-1}, 207 mV dec^{-1} and 182 mV dec^{-1} respectively as shown in Fig. 8. The low value in Tafel slope is desirable for the catalyst with fast charge transfer mechanism in glycerol electrooxidation reaction. It is evident that mixed metal oxide of nickel and cobalt (NiCoO$_2$) shows better electrooxidation reaction when compared to the individual metal oxides. Similar to Tafel slope, the two other significant parameter that determine the activity of catalysts toward electrooxidation reaction are charge transfer coefficient and exchange current density. At lower temperature, the dissociative adsorption of glycerol is considered to be the rate determining step in electrochemical glycerol oxidation, which implies that the formation of glyceraldehyde is the dominating reaction at the onset potential proceeding before the main oxidation peak.[9,38] The rate determining step in glycerol electrooxidation is one electron transfer process where the value of n in Equation 11 is considered nearly to be unity (n = 1),[39] thus the charge transfer coefficient (α) for the glycerol electrooxidation on NiO, Co$_3$O$_4$ and NiCoO$_2$ is calculated as 0.24, 0.2613 and 0.314 respectively. The extrapolation of tafel plot to the point where the potential is zero corresponds to the exchange current density and the calculated values for NiO, Co$_3$O$_4$ and NiCoO$_2$ are 13.6×10^{-6} A cm^{-2}, 9.02×10^{-6} A cm^{-2}, 42×10^{-5} A cm^{-2} respectively. The exchange current value and charge transfer coefficient is higher for NiCoO$_2$ when compared with its monometals.

Fig. 9a shows the linear sweep voltammetry (LSV) curves of glycerol electrooxidation in 1M KOH + 0.1M glycerol solution for NiO/C, Co$_3$O$_4$/C and NiCoO$_2$/C electrodes at a scan rate of 5 mVs^{-1}. The peak
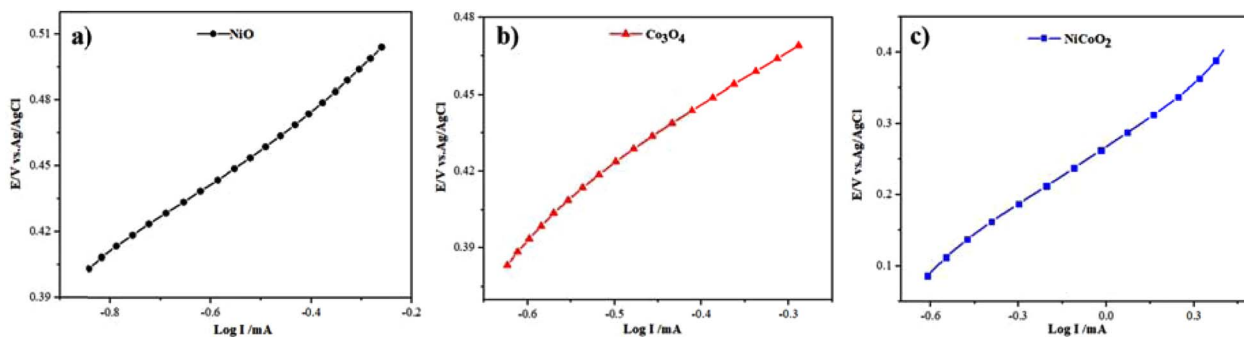
Figure 8. Tafel plot of glycerol electrooxidation in 0.1 M Glycerol + 1 M KOH at a scan rate of 50 mVs^{-1} in a) NiO/C, b) Co$_3$O$_4$/C, and c) NiCoO$_2$/C.
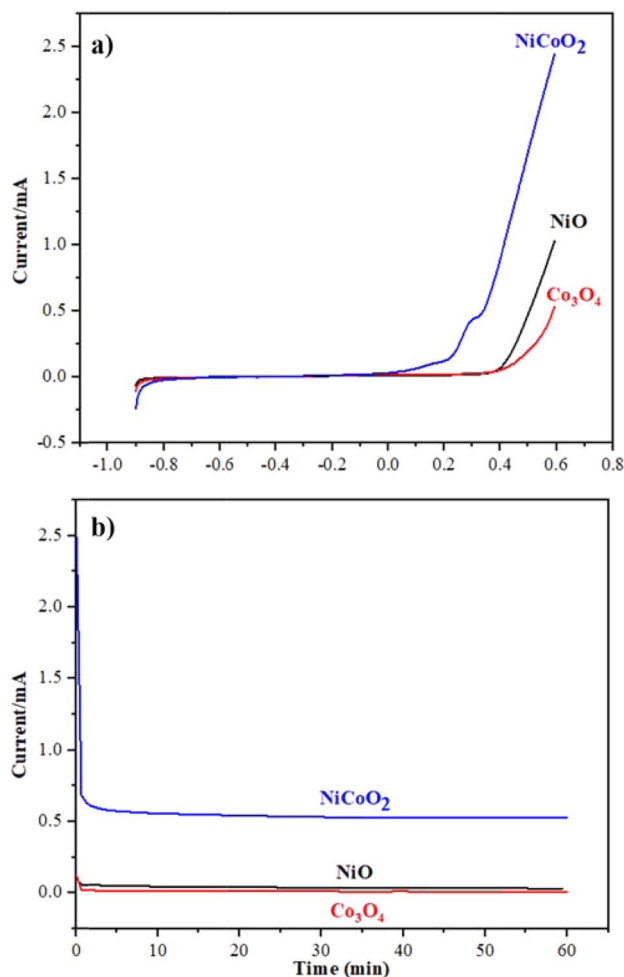

Figure 9. a) Linear sweep voltammetry (LSV) curves at 300 rpm with 5 mVs^{-1} in the potential range of −0.9 V to 0.6 V, and b) Chronoamperometric (CA) curve at 0.4 V recorded in 1M KOH + 0.1M Glycerol.

Table I. Comparison of NiCo catalyst synthesized using CS in this work with other catalyst in terms of onset potential.

Catalyst	Synthesis route	Onset potential	Ref
NiCoO$_2$	Combustion synthesis	0.09 V vs Ag/AgCl	In this work
Ni	—	0.44 V vs Hg/HgO	20
Co$_3$O$_4$	Electrodeposition	0.35 V vs Hg/HgO	41
Ni–Co/CCE	Electrochemical route	0.219 V vs SCE	19
NiCo/C	Impregnation	1.1 V vs RHE	18
AuAg/C	Colloidal route	0.72 V vs RHE	42
Pd$_{60}$Ag$_{40}$/C	Bromide anion exchange	0.5 V vs RHE	43
Ag	Melting Ag wire	0.7 V vs RHE	44

trodes toward the glycerol oxidation at 0.4 V for 60 minutes are shown in Fig. 9b. The oxidation current for NiCoO$_2$/C is larger than other two electrodes and are in good agreement with cyclic voltammetry and linear sweep voltammetry. These results indicate the synergistic effect of nickel and cobalt oxides in the mixed NiCoO$_2$ oxides with excellent activity for glycerol oxidation, better steady state electrolysis and storage properties in alkaline medium. In 2011, Gomes and co-workers used polycrystalline Pt for the electrooxidation of glycerol and identified the formation of tartronic acid, glycolic acid, glyoxylic acid, formic acid, and carbon dioxide, independent of the solution pH with an onset potential of 0.5 V vs RHE.[40] To assure the performance of NiCoO$_2$ in DAFC, the catalyst was tested for the electrooxidation reaction of ethylene glycol, ethanol and methanol and the catalysts was found to have good activity in presence all the three alcohols as shown in Fig. 10. Also, it can be seen that, the anodic and cathodic peak currents increase with scan rate with a positive shift in anodic current and negative shift in cathodic current as we discussed in the previous section. The current densities (Fig. 10) indicate the activity of the catalyst is in the order of ethanol > methanol > ethylene glycol. Based on the activity results, we can safely say that NiCoO$_2$ is a promising catalyst for alcohol fuel cells. Table I shows the comparison of NiCo catalyst synthesized using CS in this work with other catalyst in terms of onset potential.

Conclusions

Solution combustion synthesis was used for the preparation of high purity porous NiCoO$_2$ in single step. XRD pattern shows the presence of characteristic peaks corresponding to crystal planes with cubic NiCoO$_2$ phase. TEM analysis and elemental phase mapping show the presence of Ni, Co and O well dispersed and uniformly present throughout the volume of the sample. The detailed EDS analysis of Ni-Co together with the phase mapping indicate the presence of Ni and Co in equal proportion. The electrocatalytic results indicate that NiCoO$_2$ significantly improves the activity in the electrooxidation of glycerol as compared to individual oxides of nickel and cobalt. NiCoO$_2$ shows

current and the onset potential indicate the activity of electrodes toward electrooxidation. At 0.6 V, the peak current for NiCoO$_2$ is 2.5 mA and that of NiO and Co$_3$O$_4$ is 1.2 and 0.56 mA respectively. This indicates that the presence of NiCoO$_2$ increases the current approx. by two times than NiO and 4.5 times than the Co$_3$O$_4$. The results clearly indicate that the electrooxidation of glycerol on NiCoO$_2$ surface starts at a much lower positive potential than the other two electrodes. The chronoamperometric (CA) profiles providing the stability of the elec-
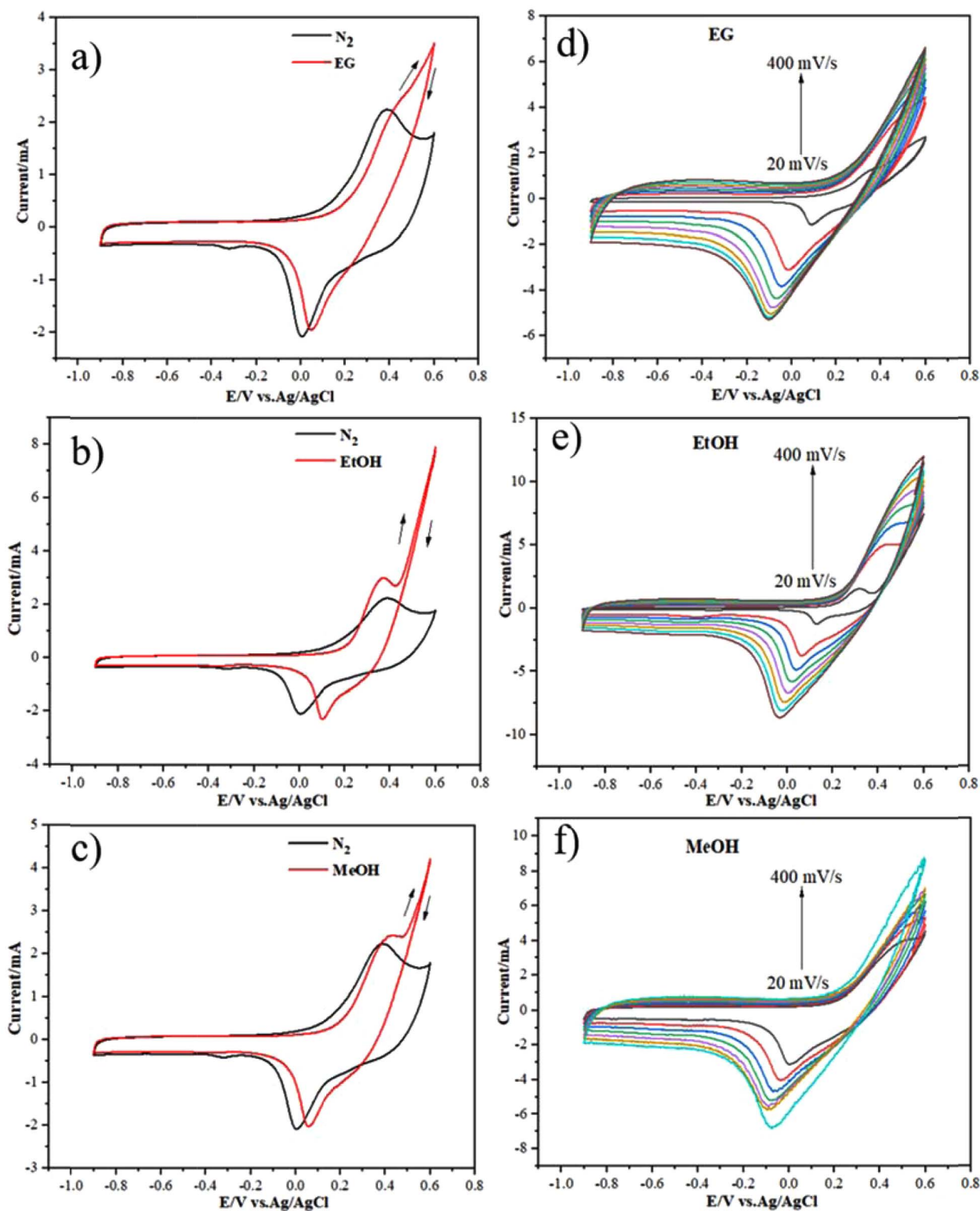
Figure 10. Cyclic voltammogram of $NiCoO_2$ to evaluate the catalytic performance of a) Ethylene Glycol b) Ethanol c) Methanol toward electrooxidation reaction and (d-f) shows the effect of scan rate on its corresponding electrooxidation.

high forward peak current density, lower onset potential and high stability at a constant voltage. The synergetic effect between nickel and cobalt is expected to modify the surface property and electronic structure of the catalysts that in-turn improves the electrocatalytic activity.

ORCID

Anand Kumar https://orcid.org/0000-0002-9146-979X

References

1. M. Matin, A. Kumar, R. Bhosale, M. S. Saad, F. Almomani, and M. Al-Marri, PdZn nanoparticle electrocatalysts synthesized by solution combustion for methanol oxidation reaction in an alkaline medium, *RSC Advances*, **7**, 42709 (2017).
2. M. A. Matin, A. Kumar, Saad Mohammed Ali, H. Saleh, M. J. Al-Marri, and S. Suslov, Zn-enriched PtZn nanoparticle electrocatalysts synthesized by solution combustion for ethanol oxidation reaction in an alkaline medium, *MRS Communications*, **8**, 411 (2017).
3. S. Sun and Z. J. Xu, Composition dependence of methanol oxidation activity in nickel–cobalt hydroxides and oxides: an optimization toward highly active electrodes, *Electrochim. Acta*, **165**, 56 (2015).
4. S. C. Chang, Y. Ho, and M. J. Weaver, Applications of real-time FTIR spectroscopy to the elucidation of complex electroorganic pathways: electrooxidation of ethylene glycol on gold, platinum, and nickel in alkaline solution, *J. Am. Chem. Soc.*, **113**, 9506 (1991).
5. A. Falase, K. Garcia, C. Lau, and P. Atanassov, Electrochemical and in situ IR characterization of PtRu catalysts for complete oxidation of ethylene glycol and glycerol, *Electrochemistry Communications*, **13**, 1488 (2011).
6. A. Falase, M. Main, K. Garcia, A. Serov, C. Lau, and P. Atanassov, Electrooxidation of ethylene glycol and glycerol by platinum-based binary and ternary nano-structured catalysts, *Electrochim. Acta*, **66**, 295 (2012).
7. M. A. Dasari, P. Kiatsimkul, W. R. Sutterlin, and G. J. Suppes, Low-pressure hydrogenolysis of glycerol to propylene glycol, *Applied Catalysis A: General*, **281**, 225 (2005).
8. B. Katryniok, H. Kimura, E. Skrzyńska, J. Girardon, P. Fongarland, M. Capron, R. Ducoulombier, N. Mimura, S. Paul, and F. Dumeignil, Selective catalytic oxidation of glycerol: perspectives for high value chemicals, *Green Chem.*, **13**, 1960 (2011).
9. Y. Kwon, K. J. P. Schouten, and M. T. Koper, Mechanism of the catalytic oxidation of glycerol on polycrystalline gold and platinum electrodes, *ChemCatChem.*, **3**, 1176 (2011).
10. N. Dimitratos, J. A. Lopez-Sanchez, S. Meenakshisundaram, J. M. Anthonykutty, G. Brett, A. F. Carley, S. H. Taylor, D. W. Knight, and G. J. Hutchings, Selective formation of lactate by oxidation of 1, 2-propanediol using gold palladium alloy supported nanocrystals, *Green Chem.*, **11**, 1209 (2009).
11. W. C. Ketchie, M. Murayama, and R. J. Davis, Selective oxidation of glycerol over carbon-supported AuPd catalysts, *Journal of catalysis*, **250**, 264 (2007).
12. Y. Kim, H. Kim, and W. B. Kim, PtAg nanotubes for electrooxidation of ethylene glycol and glycerol in alkaline media, *Electrochemistry Communications*, **46**, 36 (2014).
13. W. Hong, J. Wang, and E. Wang, Synthesis of hollow PdRuCo nanoparticles with enhanced electrocatalytic activity, *RSC Advances*, **5**, 46935 (2015).
14. M. Gao, X. Liu, M. Irfan, J. Shi, X. Wang, and P. Zhang, Nickle-cobalt composite catalyst-modified activated carbon anode for direct glucose alkaline fuel cell, *Int. J. Hydrogen Energy*, **43**, 1805 (2018).
15. O. Moradlou, H. Ansarinejad, M. Hosseinzadeh, and H. Kazemi, High-performance solid state asymmetric supercapacitor based on electrochemically decorated 3D network-like Co$_3$O$_4$ architecture on NiO nanoworms, *J. Alloys Compounds*, **755**, 231 (2018).
16. L. Zhang, S. Zhang, K. Zhang, G. Xu, X. He, S. Dong, Z. Liu, C. Huang, L. Gu, and G. Cui, Mesoporous NiCo$_2$O$_4$ nanoflakes as electrocatalysts for rechargeable Li–O$_2$ batteries, *Chemical communications*, **49**, 3540 (2013).
17. J. Song, J. Yu, M. Zhang, Y. Liang, and C. Xu, Glycerol electrooxidation on Au/Ni core/shell three-dimensional structure catalyst, *Int. J. Electrochem Sci.*, **7**, 4362 (2012).
18. V. Oliveira, C. Morais, K. Servat, T. Napporn, G. Tremiliosi-Filho, and K. B. Kokoh, Glycerol oxidation on nickel based nanocatalysts in alkaline medium–Identification of the reaction products, *J. Electroanal Chem.*, **703**, 56 (2013).
19. B. Habibi and N. Delnavaz, Electrooxidation of glycerol on nickel and nickel alloy (Ni–Cu and Ni–Co) nanoparticles in alkaline media, *RSC Advances*, **6**, 31797 (2016).
20. M. S. Houache, E. Cossar, S. Ntais, and E. A. Baranova, Electrochemical modification of nickel surfaces for efficient glycerol electrooxidation, *J. Power Sources*, **375**, 310 (2018).
21. A. Ashok, A. Kumar, R. R. Bhosale, and M. A. H. Saleh, van den Broeke, Leo JP, Cellulose assisted combustion synthesis of porous Cu–Ni nanopowders, *RSC Advances*, **5**, 28703 (2015).
22. A. Ashok, A. Kumar, R. R. Bhosale, M. A. H. Saleh, U. K. Ghosh, M. Al-Marri, F. A. Almomani, M. M. Khader, and F. Tarlochan, Cobalt oxide nanopowder synthesis using cellulose assisted combustion technique, *Ceram. Int.*, **42**, 12771 (2016).
23. A. Ashok, A. Kumar, R. R. Bhosale, F. Almomani, S. S. Malik, S. Suslov, and F. Tarlochan, Combustion synthesis of bifunctional LaMO$_3$ (M = Cr, Mn, Fe, Co, Ni) perovskites for oxygen reduction and oxygen evolution reaction in alkaline media, *J. Electroanal Chem.*, **809**, 22 (2018).
24. A. Kumar, A. Ashok, R. R. Bhosale, M. A. H. Saleh, F. A. Almomani, M. Al-Marri, M. M. Khader, and F. Tarlochan, In situ DRIFTS Studies on Cu, Ni and CuNi catalysts for Ethanol Decomposition Reaction, *Catalysis Letters*, **146**, 778 (2016).
25. A. Ashok, A. Kumar, M. A. Matin, and F. Tarlochan, Synthesis of Highly Efficient Bifunctional Ag/Co$_3$O$_4$ Catalyst for Oxygen Reduction and Oxygen Evolution Reactions in Alkaline Medium, *ACS Omega*, **3**, 7745 (2018).
26. A. Ashok, A. Kumar, R. R. Bhosale, F. Almomani, Mohd Ali H Saleh Saad, S. Suslov, and F. Tarlochan, Influence of fuel ratio on the performance of combustion synthesized bifunctional cobalt oxide catalysts for fuel cell application, *Int. J. Hydrogen Energy*, (2018).
27. A. Ashok, A. Kumar, R. Bhosale, M. A. S. Saad, F. AlMomani, and F. Tarlochan, Study of ethanol dehydrogenation reaction mechanism for hydrogen production on combustion synthesized cobalt catalyst, *Int. J. Hydrogen Energy*, **42**, 23464 (2017).
28. R. Ding, L. Qi, M. Jia, and H. Wang, Facile and large-scale chemical synthesis of highly porous secondary submicron/micron-sized NiCo$_2$O$_4$ materials for high-performance aqueous hybrid AC-NiCo$_2$O$_4$ electrochemical capacitors, *Electrochim. Acta*, **107**, 494 (2013).
29. Y. Yang, M. Zhou, W. Guo, X. Cui, Y. Li, F. Liu, P. Xiao, and Y. Zhang, NiCoO$_2$ nanowires grown on carbon fiber paper for highly efficient water oxidation, *Electrochim. Acta*, **174**, 246 (2015).
30. D. U. Lee, B. J. Kim, and Z. Chen, One-pot synthesis of a mesoporous NiCo$_2$O$_4$ nanoplatelet and graphene hybrid and its oxygen reduction and evolution activities as an efficient bi-functional electrocatalyst, *Journal of Materials Chemistry A*, **1**, 4754 (2013).
31. E. Umeshbabu, G. Rajeshkhanna, P. Justin, and G. R. Rao, Synthesis of mesoporous NiCo$_2$O$_4$–rGO by a solvothermal method for charge storage applications, *RSC Advances*, **5**, 66657 (2015).
32. S. K. Meher and G. R. Rao, Ultralayered Co$_3$O$_4$ for high-performance supercapacitor applications, *The Journal of Physical Chemistry C*, **115**, 15640 (2011).
33. X. Tang, B. Zhang, C. Xiao, H. Zhou, X. Wang, and D. He, Carbon nanotube template synthesis of hierarchical NiCoO$_2$ composite for non-enzyme glucose detection, *Sensors Actuators B: Chem.*, **222**, 232 (2016).
34. R. Sun, Y. Zhang, Y. Tang, Y. Li, S. Ding, and X. Liu, NiCoO$_2$ nanosheets grown on nitrogen-doped porous carbon sphere as a high-performance anode material for lithium-ion batteries, *Int. J. Hydrogen Energy*, **42**, 13150 (2017).
35. M. Fleischmann, K. Korinek, and D. Pletcher, The oxidation of organic compounds at a nickel anode in alkaline solution, *Journal of Electroanalytical Chemistry and Interfacial Electrochemistry*, **31**, 39 (1971).
36. A. El-Shafei, Electrocatalytic oxidation of methanol at a nickel hydroxide/glassy carbon modified electrode in alkaline medium, *J. Electroanal Chem.*, **471**, 89 (1999).
37. G. Vertes and G. Horanyi, Some problems of the kinetics of the oxidation of organic compounds at oxide-covered nickel electrodes, *Journal of Electroanalytical Chemistry and Interfacial Electrochemistry*, **52**, 47 (1974).
38. T. Holm, P. K. Dahlstrøm, O. S. Burheim, S. Sunde, D. A. Harrington, and F. Seland, Method for studying high temperature aqueous electrochemical systems: Methanol and glycerol oxidation, *Electrochim. Acta*, **222**, 1792 (2016).
39. V. Oliveira, C. Morais, K. Servat, T. Napporn, G. Tremiliosi-Filho, and K. Kokoh, Studies of the reaction products resulted from glycerol electrooxidation on Ni-based materials in alkaline medium, *Electrochim. Acta*, **117**, 255 (2014).
40. J. F. Gomes and G. Tremiliosi-Filho, Spectroscopic studies of the glycerol electrooxidation on polycrystalline Au and Pt surfaces in acidic and alkaline media, *Electrocatalysis*, **2**, 96 (2011).
41. S. Sun, L. Sun, S. Xi, Y. Du, M. A. Prathap, Z. Wang, Q. Zhang, A. Fisher, and Z. J. Xu, Electrochemical oxidation of C3 saturated alcohols on Co$_3$O$_4$ in alkaline, *Electrochim. Acta*, **228**, 183 (2017).
42. A. G. Garcia, P. P. Lopes, J. F. Gomes, C. Pires, E. B. Ferreira, R. G. Lucena, L. H. Gasparotto, and G. Tremiliosi-Filho, Eco-friendly synthesis of bimetallic AuAg nanoparticles, *New Journal of Chemistry*, **38**, 2865 (2014).
43. Y. Holade, C. Morais, S. Arrii-Clacens, K. Servat, T. Napporn, and K. Kokoh, New preparation of PdNi/C and PdAg/C nanocatalysts for glycerol electrooxidation in alkaline medium, *Electrocatalysis*, **4**, 167 (2013).
44. N. Y. Suzuki, P. V. Santiago, T. S. Galhardo, W. A. Carvalho, J. Souza-Garcia, and C. A. Angelucci, Insights of glycerol electrooxidation on polycrystalline silver electrode, *J. Electroanal Chem.*, **780**, 391 (2016).